Colloid Polym Sci 274:93–104 (1996)

LEADING CONTRIBUTION

T. Okubo
K. Kiriyama
N. Nemoto
H. Hashimoto

Static and dynamic light-scattering of colloidal gases, liquids and crystals

Received: 18 April 1995
Accepted: 22 September 1995

Prof. Dr. T. Okubo[1] (✉) · K. Kiriyama
Department of Polymer Chemistry
Kyoto University
Kyoto 606-01, Japan

N. Nemoto · H. Hashimoto
Department of Applied Physics
Kyushu University Fukuoka 812, Japan

[1] *Current address*:
Department of Applied Chemistry
Faculty of Engineering, Gifu University
Gifu 501-11, Japan

Abstract Static and dynamic light–scattering measurements are made for colloidal-crystals, -liquids and -gases of silica spheres, 103 nm in diameter, in the exhaustively deionized suspension and in the presence of sodium chloride. Sharp peaks in the scattering curve are observed, for the first time, for the colloidal crystals in very diluted aqueous suspension. The product of the effective diffusion coefficient and the scattered light intensity is found constant over the whole range of the scattering angle measured for the colloidal crystals and liquids. Three and two dynamic processes have been extracted separately from time profiles of autocorrelation function of colloidal crystals and liquids, respectively from Marquadt histogram analysis. Decay curves of colloidal gases are characterized by a single translational diffusion coefficient, D_0. D_0 of the gases is always lower than the calculation from the Stokes–Einstein equation with the true diameter of spheres, and increases as ionic concentration increases. These experimental results emphasize the important role of the expanded electrical double layers on the diffusive properties in the colloidal crystals, liquids and gases.

Key words Dynamic light-scattering – static light-scattering – colloidal crystals – electrical double layer – silica spheres

Introduction

Colloidal suspensions, especially in the *completely deionized* condition, display crystal-like distributions called *colloidal crystals* [1–16]. Surprisingly, morphology and growing mechanism of the colloidal single crystals are quite similar to those of metals, proteins and other kinds of crystals. However, forces responsible for the formation of colloidal crystals seem to be different from other crystals. Expanded electrical double layers and the electrostatic interparticle *repulsive* interactions are essential for the former, whereas some kinds of attractive interactions between the constituent materials are important for the latter. Generally speaking, critical concentration of melting for the colloidal crystals is very low, i.e., around 0.0002 in volume fraction in the deionized state. Furthermore, interparticle distance corresponding to the critical concentration is very long, on the order of several hundreds to thousands nanometers for the colloidal particles of 100 nm in diameter, for example. In these circumstances, at a first glance, we need some kinds of interparticle attraction for crystallization. However, it should be noted that the effective concentration of particles including the *expanded electrical double layers*, which moves always with the particles, is substantially high, even close to the close-packing concentration of 0.74 in volume fraction. Thus, respective particles in colloidal crystals

Colloid & Polymer Science, Vol. 274, No. 2 (1996)

interact very strongly and further in a cooperative manner just like spheres in the highly *concentrated* suspension through the double layers by the electrostatic *repulsive* forces. Interparticle attraction hypothesis has been proposed by Ise et al. from the erroneous experiments where the particles in suspension are sedimented in part by the gravity [12]. Thus, their hypothesis is in our opinion doubtful. Study on the dynamic characters of such a highly diluted but effectively highly concentrated suspension is very important for the understanding of the formation mechanism of colloidal crystals including morphology and mechanism of nucleation and crystal growth.

Static (SLS) and dynamic light scattering (DLS) techniques are now some of the most familiar methods for determining sphere diameter, and also for study of the structural and dynamic characters of colloidal suspension. Several researchers have reported the characteristics in the diffusive properties of charged colloidal spheres in dilute suspension [16–23]. However, only a few SLS and DLS studies on the structured suspensions, especially on the *crystal-like* structures in the *exhaustively deionized* aqueous suspensions have been reported hitherto [24–26], although DLS of the highly concentrated dispersions in non-aqueous solvents has been studied [27]. It should be noted that the critical concentration of melting in the completely deionized suspension is low, 0.0002 in volume fraction as described above. Furthermore, turbidity of the liquid-like and crystal-like suspensions is fairly low compared with that of gas-like suspensions due to the greatly diminished intensity of the multiple scattering for visible light. Recently, very large size of (giant) single crystals have been formed for the diluted and exhaustively deionized suspensions [28–30]. For these suspensions, turbidity was fairly low. Thus, dynamic light scattering measurements for the colloidal crystals and liquids are performed, surprisingly, rather easily.

Another purpose of this work is to ascertain the important role of the electrical double layers for the diffusion of colloidal spheres in gas-like structure. Several years ago, we reported the extraordinary translational-diffusion behavior of colloidal spheres in deionized suspension by using a metallurgical microscope [31]. The translational diffusion coefficient of polystyrene spheres, 120 nm in diameter, decreased sharply as NaCl concentration decreased. However, this peculiar observation, at first glance, was explained nicely with the role of the electrical double layers. Quite recently, from the measurements of sedimentation velocity of silica spheres and heavy polystyrene spheres, we ascertained the important role of the electrical double layers on the translational diffusion of colloidal spheres in the exhaustively deionized suspension [32]. Furthermore, the rotational diffusion coefficients of ellipsoidal colloids of tungstic acid [33] and poly (tetrafluoroethylene) [34] colloids decreased as the ionic concentration of suspension decreased, which was also explained beautifully with the expanded electrical double layers.

Experimental

Materials

Colloidal silica spheres of CS-81 was a gift from Catalyst & Chemicals Ind. Co. (Tokyo). Diameter (d_0), standard deviation (δ) from the mean diameter, and polydispersity index (δ/d_0) where 103 nm, 13.2 nm, and 0.13, respectively. The values of d_0 and δ were determined from an electron microscope. The charge density of the spheres was determined by conductometric titration with a Wayne–Kerr autobalance precision bridge, model B331, mark II (Bogner Regis, Sussex). Charge density of strongly acidic groups was 0.38 $\mu C/cm^2$. The sphere sample was carefully purified several times using an ultrafiltration cell (model 202, membrane: Diaflo-XM300, Amicon Co.). Then the sample was treated on a mixed bed of cation- and anion-exchange resins [Bio-Rad, AG501-X8(D), 20–50 mesh] more than 1 year before use, since the newly produced silica spheres release a considerable amount of alkali ions from sphere surfaces for a long time. Water used for the purification and for suspension preparation was deionized by using cation- and anion-exchange resins [Puric-R, type G10, Organo Co. (Tokyo)], purified by a Milli-Q reagent grade system (Millipore Co., Bedford, MA), and further treated with the ion-exchange resins of Bio-Rad.

Static (SLS) and dynamic light scattering (DLS) measurements

The SLS and DLS measurements were performed on a dynamic light scattering spectrophotometer(DLS-7000, Otsuka Electronics, Osaka). The goniometer spans from 15° to 160° in the scattering angle(θ) and a He-Ne-laser (10 mW, Uniphase Co.) was used as a light source at 633 nm. The source light was vertically polarized after passing through two pinpoint holes, and then focused on the center of the cell. A correlator was used to obtain the photon intensity autocorrelation function. The sample of 5 mL was prepared by filtering with a disposable syringe filter unit(DISMIC-25, 0.2 μm, Toyo Roshi Co. Tokyo) into a Pyrex cuvette cell(12 mm in outside diameter and 130 mm in length) with a screw cap. These cuvette cells were ground carefully in a spectroscopically guranteed

level. SLS and DLS measurements for the samples without resins have been made within 2 h after the suspension was set in the cells. However, measurements for the *deionized* suspensions with the Bio-Rad resins coexisted were made *more than* 3 *or* 4 *weeks* after the suspensions were set. Amount of resins added was always much in excess compared with the ionic impurities in suspension. Absorption of the colloidal spheres on the resins was safely neglected by the repeated mixing of the suspension. Note that it takes such a long time before attaining the *completely deionized* suspension with the coexistence of the ion-exchange resins. During the measurement the cuvette was kept under isothermal condition at $24 \pm 0.02\,^{\circ}C$ in a cylindrical vat containing silicon oil.

Data analysis was made with the cumulant and histogram methods including Marquadt analysis [35]. As will be discussed below, the autocorrelation function of scattered field, $g^{(1)}(\tau)$ is actually found to be a single exponential decaying function only for the suspension containing foreign salt and/or of "gas-like" structures. For "liquid-like" and "crystal-like" suspensions, the intersphere interaction is so strong that $g^{(1)}(\tau)$ deviates from a single exponential greatly. In these cases histogram methods including the Marquadt and the non-negative least square (NNLS) analyses were applied in this work in order to obtain the distribution of the decay rates, and then the diffusion coefficients or hydrodynamic diameters [35].

Background for Data analysis

The homodyne photoncorrelation spectroscopy measures the normalized intensity autocorrelation function $g^{(2)}(\tau)$ which is related to the autocorrelation function of the scattered field, $g^{(1)}(\tau)$ following the Gauss central-limit theorem.

$$g^{(2)}(\tau) = 1 + \beta |g^{(1)}(\tau)|^2 , \tag{1}$$

where β is the amplitude. When the suspension of monodisperse spheres is sufficiently dilute so that the intersphere interaction may be negligible, the decay of concentration fluctuation only occurs by the translational diffusion motion of a free particle. It should be mentioned here that the homodyne analysis of the scattered light from the strongly interacting systems including colloidal crystals has not been justified firmly. The $g^{(1)}(\tau)$ is represented by a single exponential type of decay function, Eq. (2), from which the translational diffusion coefficient, D_0 is easily estimated.

$$g^{(1)}(\tau) = \exp(-q^2 D_0 \tau) . \tag{2}$$

Here, q is the scattering vector whose magnitude is equal to $(4\pi/\lambda)\sin(\theta/2)$, where λ is the wavelength of the incident beam in medium. From D_0, we may calculate the hydrodynamic diameter, d_H of the sphere using the Stokes–Einstein equation,

$$d_H = k_B T / 3\pi\eta_0 D_0 . \tag{3}$$

Here η_0 is the solvent viscosity.

In the liquid-like state where the colloidal particles are locally ordered to be reflected as the maximum of the static structure factor $S(q)$ at q_m, $g^{(1)}(\tau)$ is no longer fitted by Eq. (2). In this case, the first cumulant $\Gamma_e \equiv K_1$ defined by Eq. (4) is conveniently used for characterization of dynamical behavior of the spheres in the liquid state.

$$\ln g^{(1)}(\tau) = \sum K_n (-\tau)^n / n! . \tag{4}$$

The Γ_e was found proportional to $S(q)^{-1}$ as predicted by the theory. For $q \gg q_m$ where $S(q) \cong 1$, on the other hand, $g^{(1)}(\tau)$ shows the bimodal distribution of the decay rate, in which the short time diffusion coefficient is close to D_0 and the long time diffusion coefficient D_1 is smaller than D_0 by a factor of about 3 [36]. The short time behavior represents the Brownian motion of the particle in a cage formed by neighboring particles, and the behavior at the long time end (much) longer than the life time of the cage, τ_1, according to the notation by Pusey, represents diffusion through several nearest-neighbor cages.

When the suspension is completely deionized, the colloidal crystal is formed [37], and DLS proves the overdamped motion of the particle on the lattice, which have been investigated by Hurd et al. [24], Cotter and Clark [26], and van Megen et al. [27]. For example, Cotter and Clark showed that Γ_e from thermal fluctuation with q along lattice symmetry direction was given by Eq. (5),

$$\Gamma_e(q) = \omega(q)^2 / \lambda(q) , \tag{5}$$

where $\omega(q)$ is the undamped mode frequency of harmonic ossillator and $\lambda(q)$ the damping coefficient. Equation (5) predicts that for single scattering in the harmonic approximation, Γ_e is periodic in reciprocal space, being in agreement with experiments. For DLS measurements on colloidal crystals which are randomly oriented in space the time profile of $g^{(1)}(\tau)$ is not exactly known.

Results and discussion

Importance of the electrical double layers in the formation of colloidal crystals

Ionic groups either dissociated or adsorbed on the colloidal surfaces leave their counterions in suspension, and

these excess charges accumulate near the surface forming an *electrical double layer*. The double layer consists of two regions; an inner region composed of adsorbed counterions (the Stern layer) and a diffuse region containing the remainder of the excess counterions (the Gouy–Chapman layer). The counterions in the diffuse region are distributed according to a balance between the thermal diffusive force and the forces of electrical attraction. The thickness of the diffuse layer is approximated by the Debye-screening length (l_{DH}):

$$l_{DH} = (4\pi e^2 n/\varepsilon k_B T)^{-1/2}\,, \qquad (6)$$

where e is the electronic charge, ε is the dielectric constant of the solvent, k_B is the Boltzmann constant, and n is the concentration of free-state cations and anions in suspension, and is given by $n = n_c + n_s + n_0$, where n_c is the concentration (number of ions per cm^3) of *diffusible* (or *free-state*) counterions, n_s is the concentration of foreign salt, sodium chloride, for example, and n_0 is the concentration of both H^+ and OH^- ions from dissociation of water. In order to estimate n_c, the *fraction of free counterions* must be known, since most counterions are bound tightly with the ions of the colloidal surface [1,38–41]. Note that the maximum values of l_{DH} both observed and calculated are very long, ca. 1 μm in water.

According to the effective hard-sphere model [42–48] which is a simple but very convenient assumption especially for the *deionized* colloidal suspension, crystal-like ordering is formed when the effective diameter (d_{eff}) of the spheres including the Debye-screening length is close to or larger than the intersphere distance (l), i.e., d_{eff} [diameter (d_0) + $2 \times l_{DH}$] > l. Note that the observed intersphere spacing (l) is always close to the calculated mean intersphere distance (l_0), and l_0 can be safely replaced with l except for the interfacial region of suspension with air or cell wall. The lattice spacing in the neighborhood of the interfaces is shorter than that in the bulk phase of suspension, which has been clarified by the measurements of reflection spectra, ivanescent-wave scattering, and surface tension of colloidal crystals [7, 49–51].

Light scattering curves of colloidal crystals and liquids

Figure 1 shows the static light-scattering intensity, $I(q)$ and the effective diffusion coefficients estimated from the cumulant analysis, D_{eff}, as a function of scattering vector, q for the sample with $\phi = 0.0049$. Circles and crosses indicate the data for the suspensions with and without resins coexisted. The suspensions are crystal-like and liquid-like, respectively. Surprisingly, very sharp peaks appeared for the crystals. The measurements have been made at intervals of half the degree. However, this interval was not always narrow enough for the determination of the reliable values of peak scattering vector, q_m. Similar profiles in the intensity of scattered light showing the peaks have been reported for the colloidal crystals [26, 52, 53]. However, most of the experiments were made for the much higher sphere concentrations than this work.

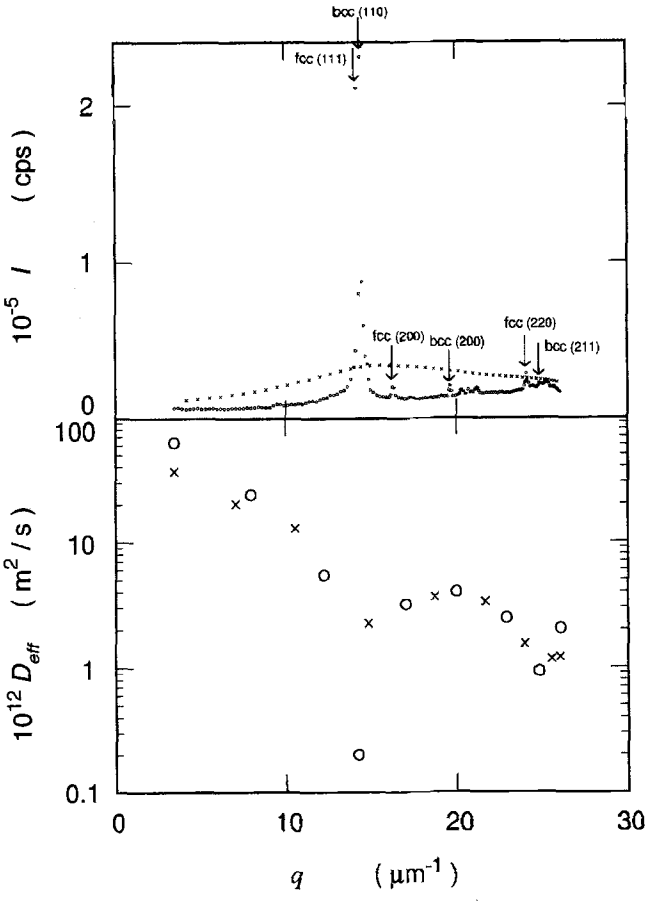

Fig. 1 Scattering intensity and diffusion coefficient as a function of scattering vector at 24 °C. $\phi = 0.0049$. *O*: with resins, for 7 days, *X*: without resins

Assignment of the respective peaks, q_m to the crystal planes was made rather easily from comparison of the observed peak vectors with the calculation from $q_{hkl} = 2\pi/a(h^2 + k^2 + l^2)^{1/2}$, where h, k and l are Miller's indices and a the unit cell size. Clearly, very sharp double peaks appeared at low q in the figure, and were assigned to be (111) and (110) reflections of face-centered cubic (*fcc*) and body-centered cubic (*bcc*) lattices, respectively. Most other peaks were also assigned rather accurately as is shown in the figure. The difference in the peak scattering vectors between the (111) reflection of *fcc* and (110) of *bcc* was only 1 degree in scattering angle. The Bragg distances (d_B) observed from the q_m values using Bragg equation,

$d_B = 2\pi/q_m$ were 422 nm and 436 nm for (111) of *fcc* and (110) of *bcc* lattices, respectively. The corresponding values calculated from the sphere concentration were 448 nm and 436 nm. The agreement of observation and calculation is excellent.

It should be noted here that the peaks are so sharp and the background intensity is quite low that there should be no significant difference between the profiles in the structure factor $S(q)$ and the intensity of scattered light $I(q)$.

$$I(q) \propto P(q)S(q) . \tag{7}$$

Here, $P(q)$ is the single-particle form factor, and can be estimated experimentally from the $I(q)$ measurements on the same suspension but in the presence of salt, for example.

The scattering curve for the colloidal suspensions without resins showed a very broad peak. This indicates that the suspension is "disordered" liquid like. The disordered liquids gave the single broad peak only, since the inter-sphere repulsive forces prevail only within a short distance. On the other hand, "ordered" liquid-like structure, which has been discussed by Hartl and Versmold in detail, has been often observed in the diluted and deionized suspension, as will be described later.

The diffusion coefficients evaluated from the cumulant analysis are also shown in Fig. 1. The background D-values decreased as the scattering vector increased, whereas the background intensity of scattered light for the crystals increased as q increased. Furthermore, the diffusion coefficients from the suspensions showing peaks in the light-scattering curve were substantially low. According to Pusey and Tough [20], the first cumulant K_1 in Eq. (4) is given by,

$$K_1 = D_0 q^2 / S(q), \tag{8}$$

where, D_0 is the diffusion coefficient for a system of non-interacting particles. Thus, the "effective diffusion coefficient", D_{eff} is given by,

$$D_{eff} = D_0 / S(q). \tag{9}$$

Constancy of $D_{eff} \times S(q)$ has been satisfactory for the colloidal liquids within experimental errors [20, 54, 55]. Figure 1 supports clearly that Eq. (9) is valid for the colloidal crystal systems.

Figure 2 shows the scattering curves for the deionized suspensions with $\phi = 0.00122$, 5 days after suspension preparation, and measured 25 and 60 min after inverted mixing of the sample, respectively. The q_m-values for the primary peaks, i.e., (111) plane of *fcc* lattice and/or (110) of *bcc* were very close to each other. However, other higher ordered peaks appeared at quite different scattering vectors to each other. This fact suggests that the crystal

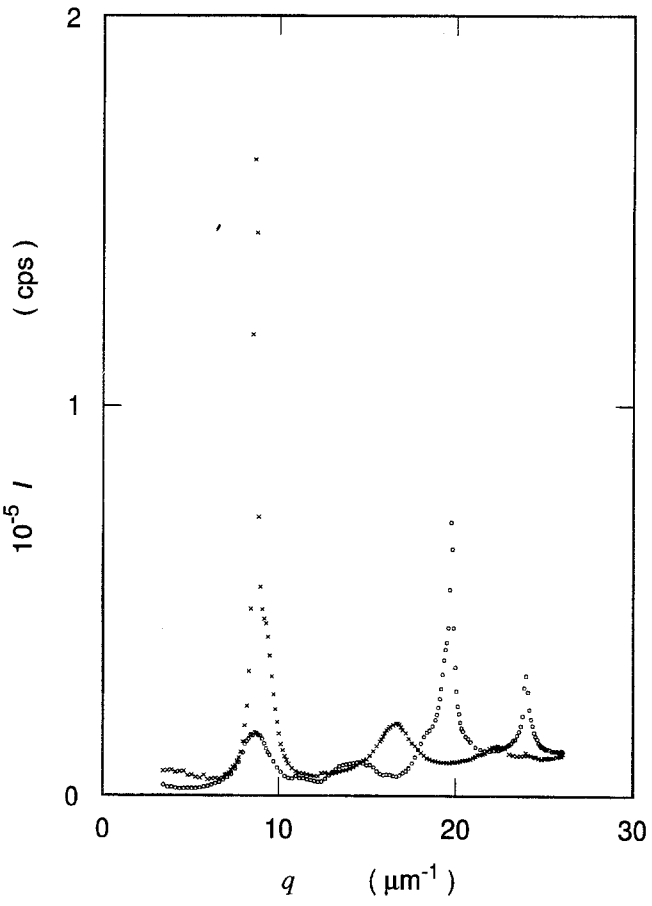

Fig. 2 Scattering intensity as a function of scattering vector at 24 °C. $\phi = 0.00122$, with resins, for 5 days. *O*: 25 min after inverted mixing, *X*: 60 min

structures are different for the two experiments. Furthermore, the primary peaks were not always highest among the peaks, which is quite different from the expectation for the powder of crystals. These observations support that the single crystals in this work are very large and directions of their crystal planes are not randomized. The lattice structures corresponding to the curves shown by open circles and crosses were assigned to be *bcc* and *fcc* lattices, respectively. Transition from *bcc* subphase to *fcc* is supported strongly with time elapsed. It is now clear that the crystal structures of colloidal crystals are *fcc* (or closed packed) and/or *bcc*. The *bcc* lattice transforms to *fcc* subphase when (a) sphere concentration is high, (b) salt concentration is lowered, (c) suspension temperature is lowered, (d) charge density of spheres is low, (e) pressure applied is low, and/or (f) time elapses after suspension preparation [3, 4, 6, 9, 11–13, 15, 56–60]. Decrease in the effective diffusion coefficients estimated from the cumulant analysis corresponded to increase in the scattering

Colloid & Polymer Science, Vol. 274, No. 2 (1996)

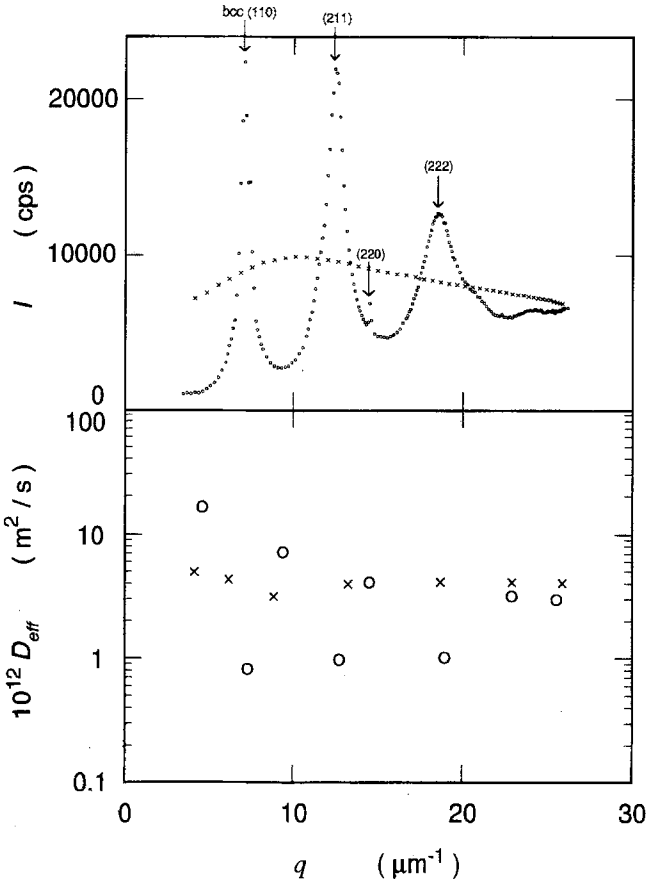

Fig. 3 Scattering intensity and diffusion coefficient as a function of scattering vector at 24 °C. $\phi = 0.000612$. *O*: with resins, for 11 days, *X*: without resins

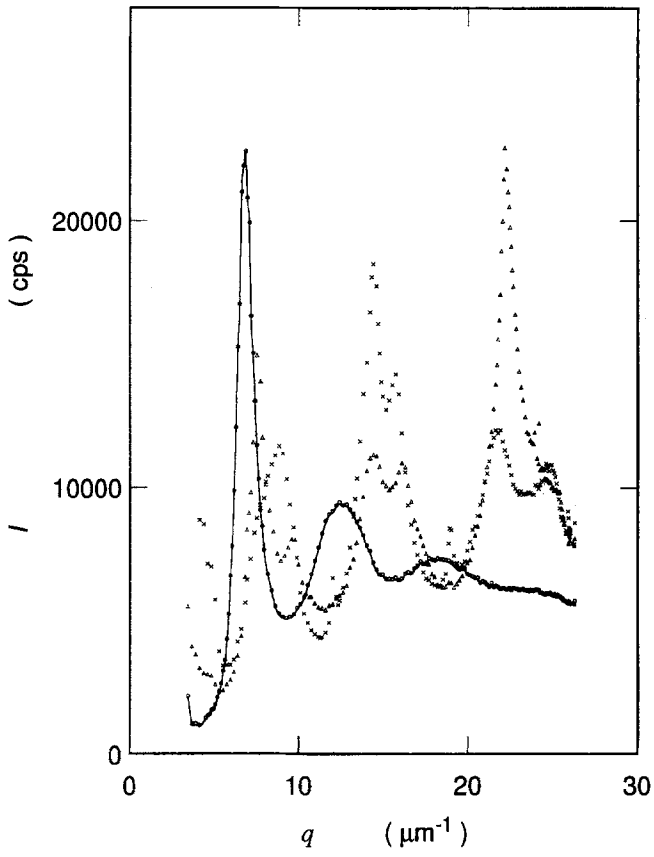

Fig. 4 Scattering intensity as a function of scattering vector at 24 °C. $\phi = 0.00049$, with resins, *O*: for 5 days, *X*: for 14 days, *Δ*: for 15 days

intensity beautifully, though the graphs showing this were omitted.

I and D_{eff} values are shown in Fig. 3 for the deionized suspension a bit higher than the critical concentration of melting, $\phi_c(=0.00046)$ [30]. The lattice structure was assigned to be *bcc* for this suspension. The Bragg distance (d_B) was estimated to be 862 nm) from the scattering vector of the primary peak, whereas d_B of *bcc* lattice was calculated as 871 nm. Agreement between observation and calculation was excellent. Constancy of the $I \times D_{eff}$ was also excellent within experimental errors.

Figure 4 shows the scattering intensities for the deionized suspension ($\phi = 0.00049$), a bit higher but very close to the $\phi_c(=0.00046)$, 12, 14 and 14 days after suspension preparation in the observation cell. Scattering curve shown by open circles is for the liquid-like suspension showing iridescent colors only. Other two curves are for the crystal-like structures showing the iridescence and very large single crystals. Crystallization occurred very sharply as the deionization reaction proceeded. Interestingly, three peaks including very sharp primary one were observed for the colloidal liquid. Liquid structure shown in the figure will be a typical example of the "super-cooled" liquids or "ordered" liquids, which has been studied in detail by Hayter et al. [61–63], Hartl and Versmold [64, 65], Ottewill [8], Klein et al. [66] and van Megen et al. [67]. However, it should be noted that sphere concentration of this work is quite low compared with these references. Interestingly, scattering curves of the crystals given by crosses and triangles in the figure showed 1st, 2nd and even 3rd series of peaks in the Bragg equation! Crystal structure was *fcc* for both curves.

I and D_{eff} values for the suspension at $\phi = 0.000294$, much below ϕ_c are shown as a function of scattering vector in Fig. 5. Typical features of the scattering curves for ordered and disordered liquids are observed clearly with and without resins, respectively. Constancy of $I \times D_{eff}$ is also rather excellent.

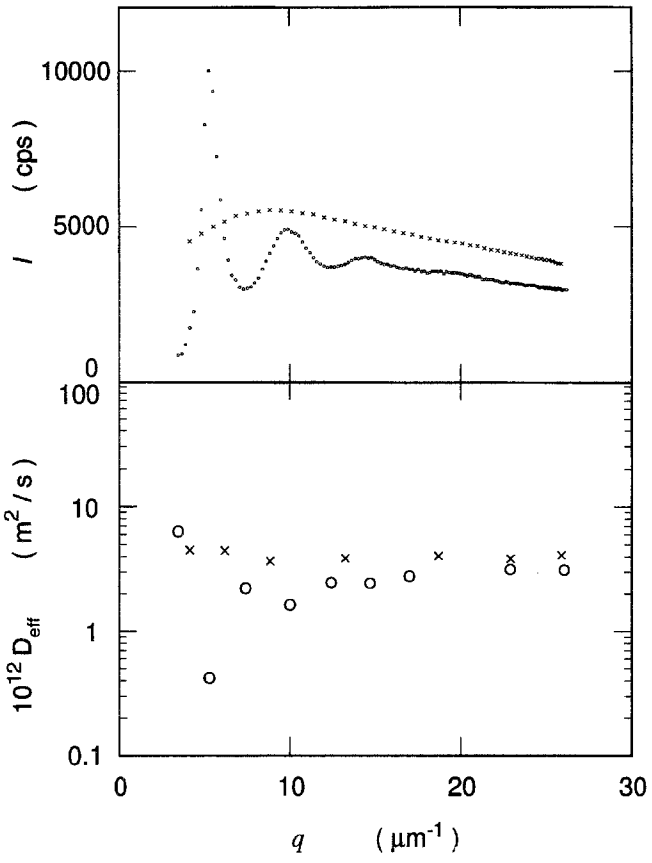

Fig. 5 Scattering intensity and diffusion coefficient as a function of scattering vector at 24 °C. $\phi = 0.000294$. *O*: with resins, for 12 days, *X*: without resins

Mode analysis of autocorrelation functions

Figure 6(a) shows a time profile of the light intensity autocorrelation function, $g^{(2)}(\tau)$ of the deionized and crystal-like suspension of silica spheres. The suspension was "crystal-like" in sphere distribution, and displayed the brilliant iridescent colors and characteristics of the beautiful single crystals. Scattering intensity often changed, rather sharply, as the cell is rotated very slowly in the cell holder of the instrument. Therefore, the observation cell was always adjusted at the position where the scattering intensity came to be minimum. This effect may be ascribed to the random directions of the refracted light through the grain boundaries or intensive light reflected on the crystal surface. The difference $\Delta g^{(2)}(\tau)$ between $g^{(2)}(\tau)$ observed and calculated from cumulant analysis is also shown in the lower part of the figure. Clearly, the observed data deviates greatly from the calculated curve with the unimodal distribution of the decay rates shown by the solid curve. This kind of deviation supports the idea strongly that there exist multi modes for the *crystal-like* suspensions.

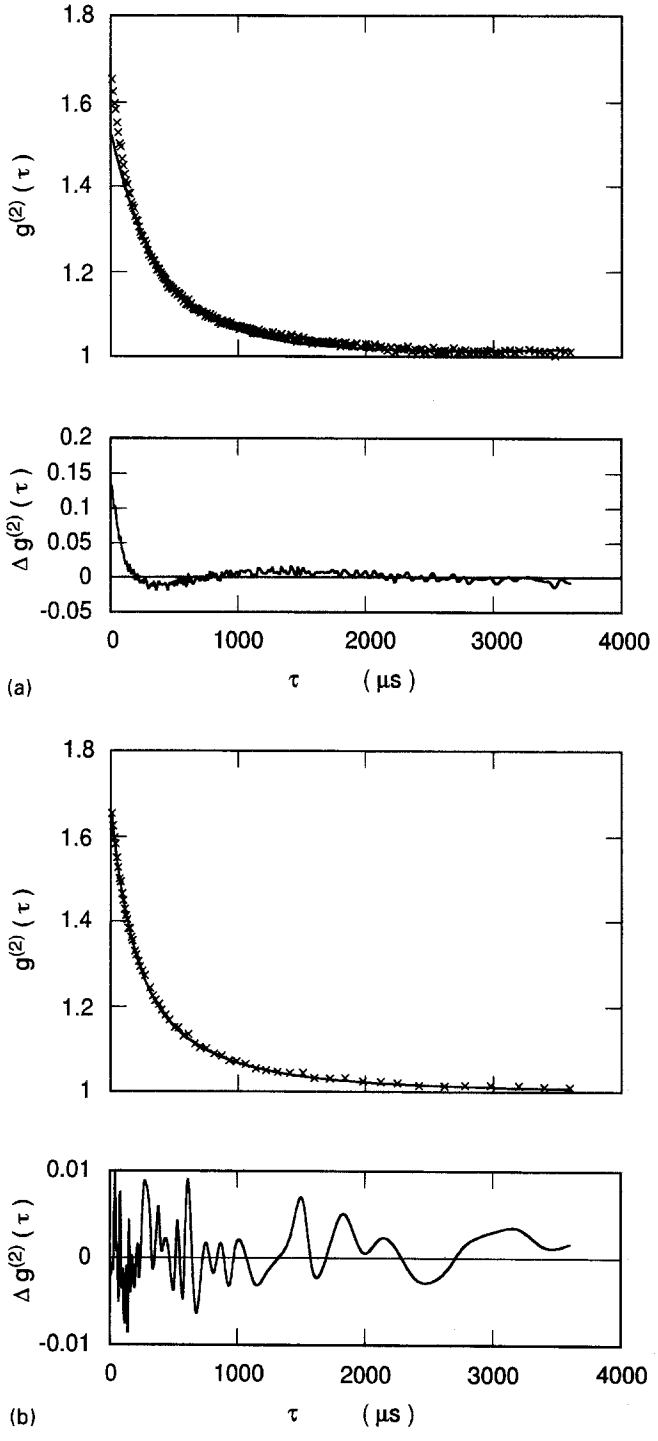

Fig. 6a) Autocorrelation function and the difference from the calculation for CS-81 spheres in the deionized suspension at 24 °C. $\phi = 0.00122$. 32 days after suspension was set in a cell. Cumulant analysis, $\theta = 90°$; **b)** Autocorrelation function and the difference from the calculation for CS-81 spheres in the deionized suspension at 24 °C. $\phi = 0.00122$. 32 days after suspension was set in a cell. Marquadt analysis, $\theta = 90°$

Separation into multi modes from these autocorrelation functions was performed by the histogram analyses of Marquadt- and non-negative least square (NNLS)-methods [35]. Figure 6(b) shows an example of data fitting by the Marquadt analysis for the DLS data given in Fig. 6(a). Clearly, the fitting was made successfully. In most cases, we adapted the Marquadt analysis mainly and occasionally the NNLS method, when we needed to ascertain the validity of the peak separation with the former analysis.

Autocorrelation functions of the *liquid-like* suspensions also have not been analyzed properly by the cumulant method, and the presence of two or rarely three modes have been confirmed by the histogram analysis, though the graphs demonstrating these were omitted here to save space. These situations were just the same as those for the crystal-like suspensions described above. Generally speaking, the difference in time profiles of the autocorrelation functions was quite tiny, unexpectedly, between "liquids" and "crystals". For the gas-like suspensions, which were obtained mainly for the very diluted suspensions or salt-containing ones, single exponential curves were observed and almost the same values of diffusion coefficients (or effective diameters) were evaluated irrespective of the analytical methods among the cumulant, Marquadt and NNLS analyses.

Dynamic character of colloidal crystals

When the suspension concentration is $\phi = 0.00049$ with ion-exchange resins (see Fig. 7), the structure changed from the gas-like to the liquid-like structure within 1 day after the suspension was set, and further to the crystal-like structure after 3 days. At $\phi = 0.0049$, crystal-like structure appeared 2 or 3 hours after suspension was set (see Fig. 8). Figures 9 and 10 show the sphere concentration dependences of the diffusion coefficients without and with resins, respectively obtained from data analysis with the cumulant method (shown by open circles and also with the Marquadt method (shown by crosses). The liquid-like structure was characterized by the short time (D_s) and long time diffusion coefficients (D_l) with $D_s = D_0$ and $D_l \cong D_s/3$. On the other hand, we found that time profiles of $g^{(2)}(t)$ of the colloidal crystal were better represented by curves fitted with three decaying components, and the results are given in terms of the apparent diffusion coefficients evaluated from respective modes, only for simplicity. Owing to our experimental setting for DLS measurements, we could neither confirm the periodic nature of the first cumulant, though the cumulant analysis resulted in a poor fit, nor calculate the decay rate from elastic constants of the colloidal crystals. Three apparent diffusion coefficients

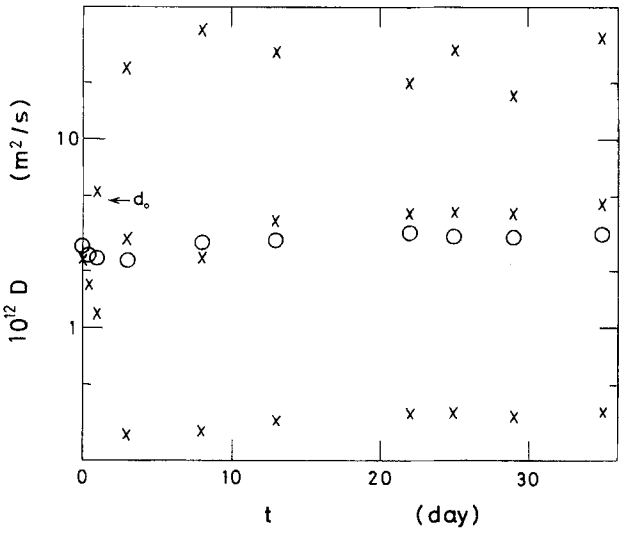

Fig. 7 Diffusion coefficient as a function of time elapsed after setting the sample with resins at 24 °C. Deionized suspensions are crystal-like. $\phi = 0.00049$. *O*: Cumulant analysis, *X*: Marquadt analysis. $\theta = 90°$

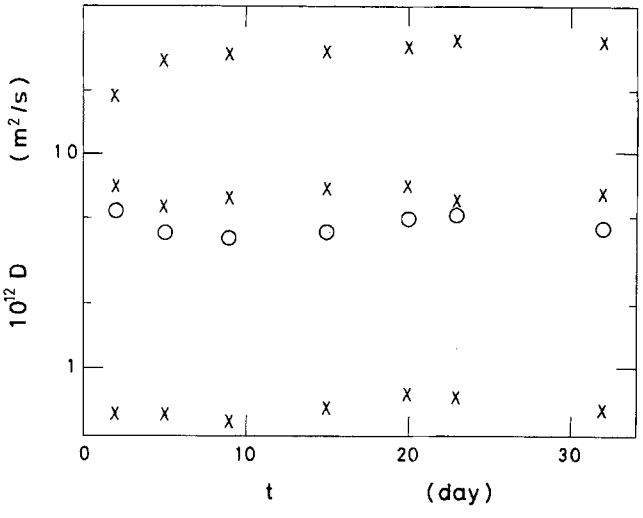

Fig. 8 Diffusion coefficient as a function of time elasped after setting the sample with resins at 24 °C. Deionized suspensions are crystal-like. $\phi = 0.0049$. *O*: Cumulant analysis, *X*: Marquadt analysis. $\theta = 90°$

($D_f > D_s > D_l$) calculated from respective rates are different by an order of magnitude to one another. Values of the fastest and the slowest modes, D_f and D_l, did not change with time once the crystal-like structure was formed, while D_s of the medium mode very gradually increased with time and became close to the intrinsic D_0 value. The medium mode, strongest in amplitude, is assigned as the Brownian

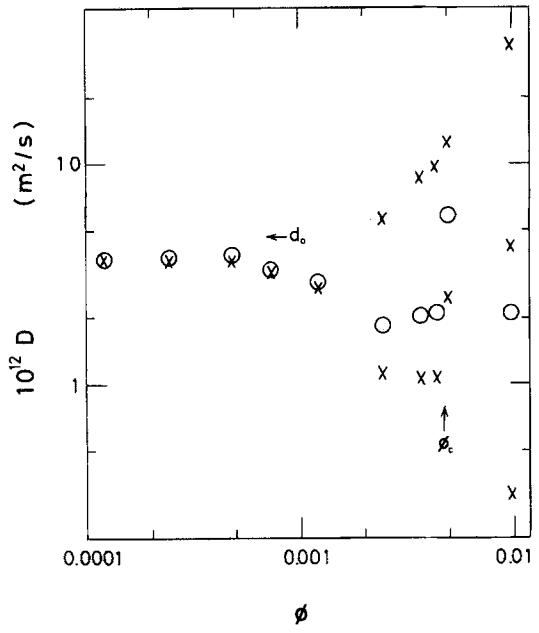

Fig. 9 Diffusion coefficient as a function of sphere concentration at 24 °C. Suspension was set without resins. d_0 and ϕ_c indicate the diameter and the critical concentration of melting, respectively. *O*: Cumulant analysis, *X*: Marquadt analysis. $\theta = 90°$

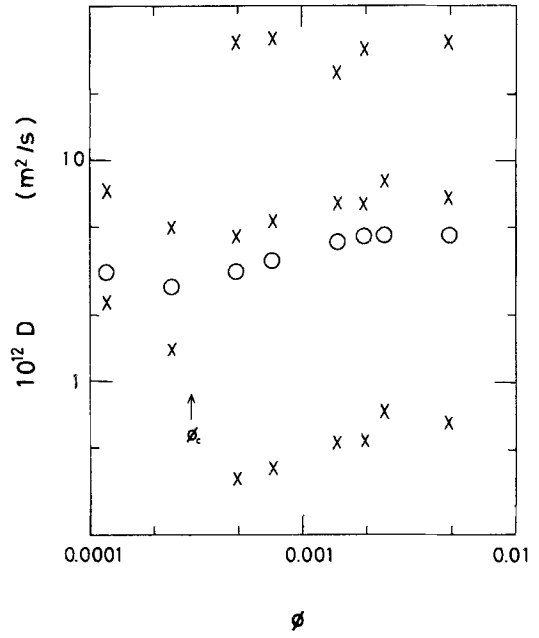

Fig. 10 Diffusion coefficient as a function of sphere concentration at 24 °C, 32 to 48 days after suspension was set with resins. d_0 and ϕ_c indicate the real sphere diameter and critical concentration of melting. *O*: Cumulant analysis, *X*: Marquadt analysis. $\theta = 90°$

oscillation of the sphere around the equilibrium lattice point, taking into account the results for the liquid-like suspension. Most impressive and exciting events in the visual observation of the crystal-like structures using a metallurgical microscope have been the synchronous movement of colloidal spheres [3, 68]. The magnitude of Brownian oscillation, $\langle\delta^2\rangle^{1/2}$ may be determined by the repulsive potential valley of crystal lattice. According to the Lindemann's law of crystal melting, the non dimensional parameter, g given by $\langle\delta^2\rangle^{1/2}/l$ (l: intersphere distance), is less than 0.1 for a stable crystal. When g equals unity the sphere distribution is ideal gas-like. The order of magnitude of the elastic modulus, G is written in terms of the magnitude of the synchronous fluctuation, δ as Eq. (10) [5, 12, 15].

$$G \cong f/l \cong (k_B T/\langle\delta^2\rangle)/l \cong N k_B T/g^2 , \tag{10}$$

where f is the elastic force constant since the magnitude of g has been estimated from the rigidities of colloidal crystals to be 0.02 to 0.1, $\langle\delta^2\rangle^{1/2}$ of spheres by the synchronous fluctuation ranges from 24 to 120 nm for $\phi = 0.00049$ for CS-81. The order of magnitude is comparable with $q^{-1} = 53.5$ nm at which our DLS experiments were performed but smaller than l_{DH}. The slowest mode cannot be assigned as the translational diffusional motion of the spheres through several nearest neighbor shells, since such a motion is prohibited in the stable crystal lattice.

Slowest mode may be related to the overdamped oscillation mode of the colloidal crystal lattice. It should be further noted here that the slowest mode is also correlated to or even corresponds to the oscillating shear waves of the elastic crystals, which has been clarified for the colloidal crystals [6, 7, 69, 70].

Concerning the fastest mode, the easiest assignment is to relate to the effect of multiple scattering. As the plot of Fig. 10 shows, D_f is, roughly speaking, independent of ϕ, and ϕ-independent amplitude to this mode may support the above idea in this relatively dilute region. However, DLS measurements on 10-times concentrated suspensions with the liquid-like structure did not show any symptom of the multiple scattering. For aqueous solutions of poly(*L*-lysine) hydrobromide with very low concentration (c_s) of added NaBr salt, the apparent D increased with decreasing c_s from 2×10^{-11} m²/s at around $c_s = 10^{-1}$ mol/dm³ to 4×10^{-10} m²/s at $c_s = 10^{-4}$ mol/dm³ [71]. This pronounced salt effect was interpreted by a theory of the electrically neutral fluctuation of local permitivity in the polyelectrolyte solutions [72]. Since the rigid silica sphere has only three degrees of freedom in comparison with a high number of internal degrees of freedom to the flexible macromolecules. The above theory may not be literally applicable for explanation of the fastest mode. However, we may not deny a possibility that the enhanced diffusion due to the interaction between charged sphere and the counter-ion clouds might be observable in the completely deionized state.

The D_s in Fig. 10 looks to increase gradually with ϕ and exceeds D_0. The d_{eff} becomes equal to l at around $\phi = 0.001$, above which the electrical double layers starts to overlap each other. Such overlapping may affect the diffusive motion of the sphere around the equilibrium position to some extent.

An increase of D_l with ϕ is noticeable and may be represented as $D_l \propto \phi^{1/3}$. The lattice dynamics predicts that the undamped frequency ω_0 with the sinusoidally varying term in Eq. (5) is proportional to the elastic constant of the lattice. Then Γ_e or D_l at constant q should be proportional to $\phi^{2/3}$ from Eq. (8), when g, the index of stability of the crystal, is independent of ϕ. More accurate measurements on ϕ dependence of G seem necessary for dilute colloidal crystals. Validity of the prediction by Cotter and Clark may have to be discussed in more detail for the suspension of the extremely low concentrations of colloidal crystals.

Colloidal single crystals are broken very easily, even by the shear stress caused by the suspension flow occurring on very small displacement of the cell. This occurs since the elastic modulus of the single crystals is extremely low [12, 16]. When the suspension displaying colloidal crystals is shaken up-and-down and left to stand, the suspension shows iridescent colors in time. Within several minutes, very small single crystals are formed and sometimes they show the blinking phenomena by the Brownian movement of the single crystals [73]. Growing process of the single crystals was observed from 10 to 40 min after shaking, and seemed to be completed after about 60 min. Figure 11 shows the preliminary results of the time dependencies of the diffusion coefficients after the suspension was mixed and put into the DLS instrument. In this figure the data point at the negative t represents the value in an equilibrium state of crystal-like suspension. Unexpectedly, the diffusive properties of the suspension do not change very much in the course of crystallization.

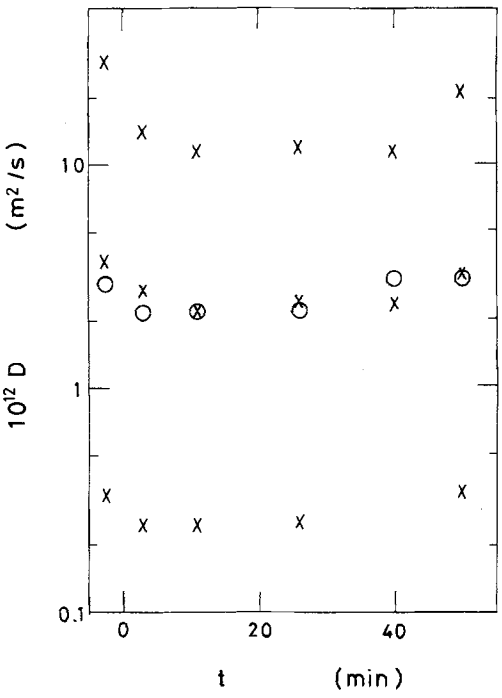

Fig. 11 Changes of diffusion coefficient in the course of crystallization at 24 °C. Mixing of suspension finished at $t = 0$. 13 days after suspension was set with resins. $\phi = 0.00049$. *O*: Cumulant analysis, *X*: Marquadt analysis. $\theta = 90°$

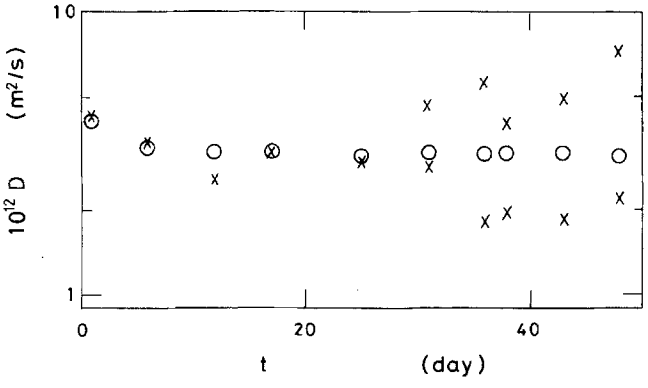

Fig. 12 Diffusion coefficient as a function of time elapsed after setting the sample with resins at 24 °C. Deionized suspensions are liquid-like. $\phi = 0.000122$. *O*: Cumulant analysis, *X*: Marquadt analysis. $\theta = 90°$

Dynamic character of colloidal liquids

Formation processes of the liquid-like structure were pursued for two suspensions at $\phi = 0.000122$ in volume fraction and 0.000245 with Bio-Rad resins coexisted in the observation cuvettes by repeated $g^{(2)}(\tau)$ measurements. It should be noted that the above two concentrations are lower than the critical concentration of melting, $\phi_c = 0.00049$ determined experimentally [30]. The $g^{(2)}(\tau)$ were analyzed with both the cumulant method and the Marquadt method to obtain the first cumulant, Γ_e and also two decay rates, from which the apparent diffusion coefficients D were evaluated. Figure 12 shows that the liquid-like structure were formed 30 days later from the gas-like one for the sample of $\phi = 0.000122$. In the gas-like suspension, the cumulant (*O*) and Marquadt (*X*) analyses gave identical single D values corresponding to the translational diffusion of free particles, which monotonically decreased with time and became constant within 30 days after setting the suspension. This means clearly that the Debye-screening

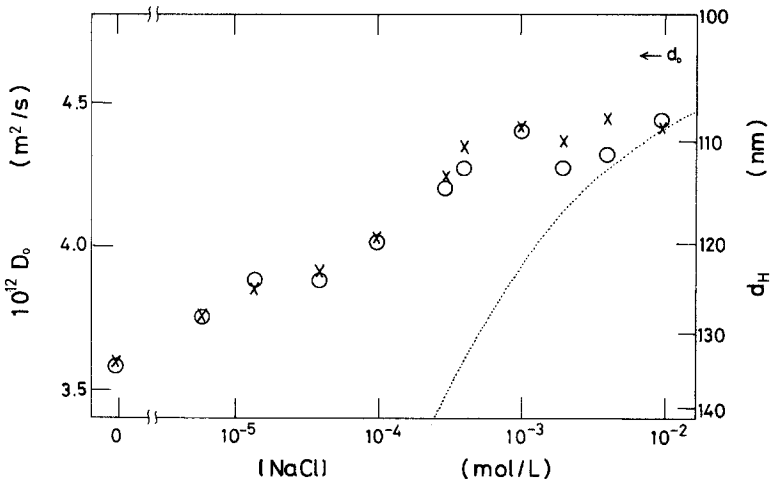

Fig. 13 Diffusion coefficient and hydrodynamic diameter as a function of ionic concentration at 24 °C. Suspensions are gas-like. $\phi = 0.00049$. *O*: Cumulant analysis, *X*: Marquadt analysis. $\theta = 90°$ Dotted curve shows the calculated values of d_{eff}

length (l_{DH}) increases in the course of deionization process with resins, and that the hydrodynamic diameter of spheres increases as the electrical double layers expands. After 30 days, the forced fit by the cumulant analysis gave D values similar to those found in the gas-like structure. However, the Marquadt analysis gives the presence of two modes to time profiles of $g^{(2)}(\tau)$. The average interparticle spacing l is calculated as 1.88×10^3 nm at $\phi = 0.000122$ using Eq. (11),

$$l = 0.904\, d_0/\phi^{1/3}(\text{nm}). \tag{11}$$

The value of scattering vector, q_m, at which $S(q)$ takes a maximum is then estimated roughly as 3.34×10^{-3} nm from $q_m \cong 2\pi/l$, which is much smaller than the q value of 1.86×10^{-2} nm at $\theta = 90°$ where our DLS measurements were made. For $q \gg q_m$, the earlier results described in the background section indicate that $g^{(2)}(\tau)$ from suspensions with the liquid-like structure is characterized by two diffusion coefficients, the short time diffusion coefficient D_s and D_l related to the long time tail of $g^{(2)}(\tau)$, being different by a factor of about 3. Our data are in good agreement with the above-mentioned results. Furthermore it is interesting to note that the D_s values are almost identical to the value calculated from the true diameter d_0 of silica sphere using Eq. (3). At $\theta = 90°$, the characteristic spacial length q^{-1} in DLS is 53.5 nm, which is much smaller than the Debye-screening length, l_{DH} estimated as 4.3×10^2 nm in the exhaustively deionized suspension. Our data suggest that the spheres make Brownian motion as if there were no characteristic interaction in small displacements during time interval in which the short-range order of the liquid-like structure is maintained. Anyway, formation of the liquid-like structure can be easily detected by DLS without knowledge of $S(q)$.

Dynamic character of colloidal gases

From the decay rate of the gas-like suspension the translational diffusion coefficient, D_0 was estimated soundly as the slope. The diffusion coefficients and the hydrodynamic diameters are displayed in Fig. 13 as a function of salt concentration. The most impressive feature in this figure is that D_0 increased significantly by 25% as concentration of sodium chloride increased. This change is explained in terms of thinning of the electrical double layers with increasing ionic concentration of suspension. Dotted curve shows the calculated value of $d_{eff}(=d_0 + 2xl_{DH})$ using Eq. (6). Good agreement between the experiment and the calculation is attained only at high concentrations of sodium chloride. Salt concentration dependency calculated is much more substantial compared with the observation. The large difference at low ionic concentrations is ascribed to the fact that the electrical double layers are soft, easily distorted, and even extinguished at one moment, and the similar situation has appeared for the viscometric properties [15]. The electrical double layers play an essential role for crystal formation at higher sphere concentration, but dynamically only a fraction of water inside the double layer moves with the sphere. Nevertheless, the hydrodynamic diameter, d_H in the deionized state is much larger than the true diameter, d_0 (103 nm) of the sphere and the greatest amount of water is contained in the shell of the thickness, $(d_H - d_0)/2 = 16$ nm. At any rate, an important contribution of the electrical double layers is not denied at all by this difference. This salt influence on the diffusion behavior strongly supports that the colloidal spheres are always accompanied by the electrical double layers and the translational movement of the former is retarded as the latter expands. It should be noted here that the observed D_0 values at high concentrations of NaCl are still lower

than that calculated from the true diameter, d_0 as is shown in Fig. 13. This may be ascribed to the hydration effect around the colloidal spheres [74]. The importance of the electrical double layers on the translational Brownian movement of colloidal spheres in gas-like suspension has been supported by other experiments [31] as was described in the Introduction section.

Acknowledgements A dynamic light-scattering spectrophotometer was purchased by a grant-in-aid from the Mitsubishi Foundation, which the authors thank sincerely. Catalyst & Chemicals Ind. Co. (Tokyo) is also thanked for kindly providing the colloidal silica sample. One of the authors (T. O.) sincerely thanks Professor Emeritus Sei Hachisu of Tsukuba University for his interest and encouragement throughout this work.

References

1. Vanderhoff W, van de Hul HJ, Tausk RJM, Overbeek JThG (1970) In: Goldfinger (ed) Clean Surfaces: Their Preparation and Characterization for Interfacial Studies. Dekker, New York
2. Hiltner PA, Papir YS, Krieger IM (1971) J Phys Chem 75:1881
3. Kose A, Ozaki M, Takano K, Kobayashi Y, Hachisu S (1973) J Colloid Interface Sci 44:330
4. Williams R, Crandall RS, Wojtowicz PJ (1976) Phys Rev Lett 37:348
5. Mitaku S, Ohtsuki T, Enari K, Kishimoto A, Okano K (1978) Jpn J Appl Phys 17:305
6. Lindsay HM, Chaikin PM 76:3774
7. Pieranski P (1983) Contemp Phys 24:25
8. Ottewill RH (1985) Ber Bunsenges Phys Chem 89:517
9. Aastuen DJW, Clark NA, Cotter LK, Ackerson BJ (1986) Phys Rev Lett 57:1733
10. Pusey PN, van Megen W (1986) Nature (London) 320:340
11. Robbins MO, Kremer K, Grest GS (1988) J Chem Phys 88:3286
12. Okubo T (1988) Acc Chem Res 21:281
13. Monovoukas Y, Gast AP (1991) Langmuir 7:460
14. Sood AK (1991) Solid State Phys 45:2
15. Okubo T (1993) Prog Polym Sci 18:481
16. Batchelor GK (1972) J Fluid Mech 52:245
17. Ohtsuki T, Okano K (1982) J Chem Phys 77:1443
18. Belloni L, Drifford M (1985) J Phys Lett 46:1183
19. Beresford-Smith B, Chan DYC, Mitchel DJ (1985) J. Colloid Interface Sci 105:216
20. Pusey PN, Tough RJA (1985) In: Pecora R (ed) Dynamic Light Scattering. Plenum, London
21. Russel WB, Saville DA, Schowalter WR (1989) Colloidal Dispersions Cambridge Univ Press, Cambridge
22. Cichocki B, Felderhof BU (1991) J Chem Phys 94:556
23. Denkov ND, Petsev DN (1992) Physica A 183:462
24. Hard AJ, Clark NA, Mockler RC, O'Sullivan WJ (1982) Phys Rev A 26:2869
25. Sasaki S, Imai N (1983) J Phys Soc Japan 52:2571
26. Cotter LK, Clark NA (1987) J Chem Phys 86:6616
27. van Megen W, Underwood SM, Pusey PN (1991) J Chem Soc Faraday Trans 87:395
28. Okubo T (1992) Naturwissenschaften 79:317
29. Okubo T (1993) Colloid Polym Sci 271:190
30. Okubo T (1994) Langmuir 10:1695
31. Okubo T (1989) J Phys Chem 93:4352
32. Okubo T (1994) J Phys Chem 98:1472
33. Okubo T (1987) J Am Chem Soc 109:1913
34. Okubo T, Shimizu T (1990) J Colloid Interface Sci 135:300
35. Lawson CL, Hansen RJ (1974) Solving Least Squares Problems. Prentice Hall, New Jersey
36. Pusey PN (1978) J Phys A 11:119
37. Schatzel K, Ackerson BJ (1993) Phys Rev E 48:3766
38. Schaefer DW (1977) J Chem Phys 66:3980
39. Alexander S, Chaikin PM, Grant P, Morales GJ, Pincus P, Hone D (1984) J Chem Phys 80:5776
40. Okubo T (1987) Ber Bunsenges Phys Chem 91:1064
41. Okubo T (1988) J Colloid Interface Sci 125:380
42. Baker JA, Henderson D (1967) J Chem Phys 47:2856
43. Wadachi M, Toda M (1972) J Phys Soc Jpn 32:1147
44. Hachisu S, Kobayashi Y, Kose A (1973) J Colloid Interface Sci 42:342
45. Brenner SL (1976) J Phys Chem 80:1473
46. Takano K, Hachisu S (1977) J Chem Phys 67:2604
47. Barnes CJ, Chan DY, Everett DH, Yates DE (1978) J Chem Soc Faraday Trans 274:136
48. Voeglli LP, Zukoski, IV CF (1991) J Colloid Interface Sci 141:79
49. Okubo T (1988) J Chem Soc Faraday Trans 1 (1988) 84:4161
50. Pouligny B, Aastuen DJW, Clark NA (1991) Phys Rev A 44:6616
51. Okubo T (1995) J Colloid Interface Sci 171:55
52. Pusey PN, van Megen W, Bartlett P, Ackerson BJ, Rarity JG, Underwood SM (1989) Phys Rev Lett 63:2753
53. von Berlepsch H, Strey R (1994) Colloid Polym Sci 272:577
54. Dalberg PS, Boe A, Strand KA, Sikkeland T (1978) J Chem Phys 69:5473
55. Gruner F, Lehmann W (1980) In: Degiorgio V, Corti M, Giglio M (eds) Light Scattering in Fluids and Macromolecular Solutions. Plenum, New York
56. Luck W, Klier M, Wesslau H (1963) Naturwissenschaften 50:485
57. Hiltner PA, Krieger IM (1969) J Phys Chem 73:2386
58. Williams R, Crandall RS (1974) Phys Lett A48:225
59. Schefer DW, Ackerson BJ (1975) Phys Rev Lett 35:1448
60. Hone D, Alexander S, Chaikin PM, Pincus P (1983) J Chem Phys 79:1474
61. Hayter JB, Penfold J (1981) Mol Phys 42:109
62. Hansen JP, Hayter JB (1982) Mol Phys 46:651
63. Snook IK, Hayter JB (1992) Langmuir 8:2880
64. Hartl W, Versmold H (1987) Z Phys Chem Neue Folge 153:1
65. Hartl W, Versmold H (1988) J Chem Phys 88:7157.
66. D'Aguanno B, Klein R (1991) J Chem Soc Faraday Trans 87:379
67. van Megen W, Underwood SM, Pusey PN (1991) Phys Rev Lett 67:1586
68. Okubo T (1989) J Chem Phys 90:2408
69. Dubois-Violette E, Pieranski P, Rothen F, Strzelecki L (1980) J Phys (Paris) 41:369
70. Stoimenova M, Okubo T (1995) J Colloid Interface Sci (in press)
71. Nemoto N, Matsuda H, Tsunashima Y, Kurata M (1984) Macromolecules 17:1731
72. Lin SC, Lee WI, Schurr JM (1978) Biopolymers 17:1041
73. Okubo T (1992) J Colloid Interface Sci 153:587
74. Sasaki S, Maeda H (1994) J Colloid Interface Sci 167:146